Altered Intersubunit Interactions in Crystal Structures of Catalytically Compromised Ribulose-1,5-bisphosphate Carboxylase/Oxygenase[†,‡]

Saeid Karkehabadi,[§] Thomas C. Taylor,[§] Robert J. Spreitzer,[||] and Inger Andersson*[,§]

Department of Molecular Biology, Swedish University of Agricultural Sciences, BMC Box 590, 751 24 Uppsala, Sweden, and Department of Biochemistry, University of Nebraska, Lincoln, Nebraska 68588-0664

Received September 24, 2004; Revised Manuscript Received October 21, 2004

ABSTRACT: Substitution of Leu290 by Phe (L290F) in the large subunit of ribulose-1,5-bisphosphate carboxylase/oxygenase from the unicellular green alga *Chlamydomonas reinhardtii* causes a 13% decrease in CO_2/O_2 specificity and reduced thermal stability. Genetic selection for restored photosynthesis at the restrictive temperature identified an Ala222 to Thr (A222T) substitution that suppresses the deleterious effects of the original mutant substitution to produce a revertant enzyme with improved thermal stability and kinetic properties virtually indistinguishable from that of the wild-type enzyme. Because the mutated residues are situated ∼19 Å away from the active site, they must affect the relative rates of carboxylation and oxygenation in an indirect way. As a means for elucidating the role of such distant interactions in Rubisco catalysis and stability, we have determined the crystal structures of the L290F mutant and L290F/A222T revertant enzymes to 2.30 and 2.05 Å resolution, respectively. Inspection of the structures reveals that the mutant residues interact via van der Waals contacts within the same large subunit (intrasubunit path, 15.2 Å Cα−Cα) and also via a path involving a neighboring small subunit (intersubunit path, 18.7 Å Cα−Cα). Structural analysis of the mutant enzymes identified regions (residues 50−72 of the small subunit and residues 161−164 and 259−264 of the large subunit) that show significant and systematically increased atomic temperature factors in the L290F mutant enzyme compared to wild type. These regions coincide with residues on the interaction paths between the L290F mutant and A222T suppressor sites and could explain the temperature-conditional phenotype of the L290F mutant strain. This suggests that alterations in subunit interactions will influence protein dynamics and, thereby, affect catalysis.

Ribulose-1,5-bisphosphate carboxylase/oxygenase (Rubisco,[1] EC 4.1.1.39) catalyzes the rate-limiting incorporation of atmospheric CO_2 into carbohydrate precursors during photosynthesis. The efficiency of this essential reaction is severely hampered by a side reaction in which atmospheric O_2 competes with CO_2 at the active site, ultimately leading to the loss of CO_2 and energy in the process of photorespiration. In addition, Rubisco is a slow catalyst with k_{cat} values of less than 10 s^{-1}. The combination of these two properties limits the rate of biomass assimilation of land plants. For these reasons, Rubisco has long been a potential target for genetic manipulation aimed at increasing the yield of crop plants (reviewed in refs *1*−*4*).

The efficiency with which CO_2 is able to compete with O_2 as the gaseous substrate can be quantified by the specificity factor $\Omega = V_cK_o/V_oK_c$, where V_c and V_o are the V_{max} values of carboxylation and oxygenation, respectively, and K_c and K_o are the K_m values for CO_2 and O_2, respectively (*5*). There is considerable variation in Ω values among Rubisco enzymes from different species. Most land plants have Ω values in the range of 80−100 (reviewed in ref *6*). The highly homologous Rubisco from *Chlamydomonas reinhardtii*, a green alga, has an Ω value of ∼60 whereas cyanobacteria and anoxic photosynthetic bacteria have values of ∼50 and ∼15, respectively (*7*). More recent investigations have identified Rubisco enzymes from nongreen algae that have Ω values in the range of 100−240 (*8*, *9*). This implies that it may be possible to engineer Rubisco enzymes from land plants with improved specificities and kinetic properties.

It has been difficult to engineer the Rubisco enzymes of land plants. Plant Rubisco is hexadecameric, consisting of eight large and eight small subunits. The large subunit is coded by a single gene in the chloroplast genome whereas the small subunit is coded by a family of closely related genes in the nucleus (reviewed in refs *10* and *11*). In addition to this genetic complexity, issues of holoenzyme folding and assembly preclude genetic manipulation of plant Rubisco in *Escherichia coli* (reviewed in ref *12*). Only recently has it become possible to transform the chloroplasts of land plants, and heterologous plant holoenzymes and a mutant large subunit have been studied in tobacco (*4*, *13*, *14*). The possibility of genetically transforming the land plant form

[†] This work was supported by grants from the Swedish Research Council for Environment, Agricultural Sciences, and Spatial Planning (FORMAS), the European Union (No. QLK3-CT-2002-01945), and the U.S. Department of Agriculture National Research Initiative (No. 2001-35318-11267).

[‡] Coordinates and structure factors have been deposited in the Protein Data Bank with accession codes 1UWA for the L290F single mutant and 1UW9 for the L290F/A222T double mutant.

* To whom correspondence should be addressed. Tel: +46-18-4714288. Fax: +46-18-536971. E-mail: inger@xray.bmc.uu.se.

[§] Swedish University of Agricultural Sciences.

[||] University of Nebraska.

[1] Abbreviations: Rubisco, ribulose-1,5-bisphosphate carboxylase/oxygenase; Ω, CO_2/O_2 specificity factor; CABP, 2-carboxy-D-arabinitol 1,5-bisphosphate; NCS, noncrystallographic symmetry.

10.1021/bi047928e CCC: $30.25
Published on Web 12/04/2004

of the enzyme opens up the possibility for using site-directed mutagenesis in order to further our understanding of the catalytic mechanism and, ultimately, to identify residues that contribute to specificity in land plant Rubisco. This approach has earlier been practiced with the prokaryotic Rubisco enzymes expressed in *E. coli* (reviewed in refs *1* and *15*). However, because of the complexity of Rubisco, it is not yet known which residues may improve Ω or carboxylation catalytic efficiency or account for differences in Ω among Rubisco enzyme from divergent species.

Genetic screening and selection in *Chlamydomonas* offer an alternative approach in which Rubisco mutants are randomly recovered on the basis of a photosynthesis-deficient phenotype (i.e., growth requirement for acetate) and subsequently defined at the molecular level. Such mutants can then be used to select for second-site mutations that restore Rubisco function and photosynthesis. Using this approach, residues in both large and small subunits, relatively far from the active site, have been identified that influence Ω (reviewed in ref *1*). The first mutant Rubisco found to have an altered Ω value was caused by a Leu290 to Phe (L290F) substitution in the chloroplast-encoded large subunit (*16*). The L290F enzyme has a 13% decrease in Ω and reduced thermal stability in vivo and in vitro (*16*, *17*). The mutant cells can grow photoautotrophically at 25 °C but lack photosynthesis and require acetate for growth at 35 °C due to the loss of Rubisco holoenzyme (*16*, *17*). Ala222 to Thr (A222T) and Val262 to Leu (V262L) second-site suppressor mutations were recovered that restored photosynthesis of the L290F mutant at the restrictive temperature (*18*). The L290F/A222T and L290F/V262L double-mutant enzymes have improved thermal stability properties and Ω values virtually indistinguishable from those of the wild-type enzyme (*18*, *19*). Here we present the first X-ray crystal structures of mutant Rubisco enzymes that have a decrease (L290F single mutant) or increase (L290F/A222T double mutant) in Ω as a result of amino acid substitutions far from the active site. These structures can explain the molecular basis for holoenzyme instability at elevated temperature and provide insight into the mechanism by which interactions between large and small subunits may influence Rubisco catalysis.

EXPERIMENTAL PROCEDURES

Protein Purification. *C. reinhardtii* cells were grown at 28 °C in darkness with acetate medium (*20*). Cells were harvested by centrifugation in 500 mL bottles at 2500*g* for 5 min and lysed by sonication. The mutant Rubisco enzymes were purified using a procedure similar to that described for the wild-type enzyme (*21*). A differential ammonium sulfate precipitation between 30% and 50% saturation was carried out. The pellet was then dissolved and loaded on a Superdex-200 16/60 size exclusion column. The fractions corresponding to Rubisco were collected and loaded onto a Mono Q anion-exchange column. Rubisco was eluted from the column with a 0.1−0.4 M NaCl gradient. The L290F single-mutant enzyme was purified in the presence of 1 mM dithiothreitol, and the L290F/A222T and L290F/V262L double-mutant enzymes were purified in the presence of 5 mM β-mercaptoethanol throughout.

Crystallization and Data Collection. Purified protein was concentrated to 10 mg/mL in an activating buffer containing 50 mM HEPES (pH 7.5), 10 mM $NaHCO_3$, and 5 mM $MgCl_2$. Crystals of the Rubisco mutants were grown using the hanging-drop vapor diffusion method at 20 °C. The drop contained equal amounts of the protein sample in activating buffer containing 1 mM carboxyarabinitol bisphosphate (CABP) and well solution consisting of 50 mM HEPES (pH 7.5), 50−200 mM NaCl, 7−12% PEG 4000, 10 mM $NaHCO_3$, and 5 mM $MgCl_2$. Crystals belonging to space group $P2_1$ appeared within 1 week (Table 1). Crystals of the mutants are significantly more mosaic than the wild-type enzyme crystals (*21*). Prior to data collection, crystals were frozen in liquid N_2 using a mother liquor with 30% ethylene glycol added as a cryoprotectant. Data for the L290F single-mutant enzyme were collected on beam line I711 at Max-lab, Lund, Sweden, and for the L290F/A222T double-mutant enzyme on beam line ID14-1 at ESRF, Grenoble, France, from single crystals at 100 K. The data were processed using DENZO and SCALEPACK (*22*) to a resolution of 2.3 Å for the single-mutant and 2.05 Å for the double-mutant enzymes. Data for L290F/V262L suffered from twinning and were not useful. The resulting merging *R*-values are generally higher for the mutant data than for wild type (*21*). This may be attributed to a combination of high mosaicity, large unit cells, and low symmetry (requiring the collection of a large number of images and data sets containing predominantly partial reflections).

Structure Determination and Refinement. The mutant crystal structures were solved by molecular replacement using the program AMORE (*23*, *24*). The search model consisted of a set of one large and one small subunit of wild-type *Chlamydomonas* Rubisco (PDB code 1GK8) in which the side chains of the substituted residues had been removed. In each case, eight solutions corresponding to eight different orientations of the search model within one hexadecamer in the asymmetric unit were found.

Table 1: Statistics for Data Collection and Refinement

	L290F	L290F/A222T
resolution limit[a] (Å)	2.3 (2.34−2.30)[d]	2.05 (2.09−2.05)
space group	$P2_1$	$P2_1$
cell dimensions		
a, *b*, *c* (Å)	121.0, 177.7, 122.7	126.0, 178.2, 120.5
β (deg)	117.7	120.5
no. of reflections		
measured	5929213	1869012
unique	197942	295370
completeness (%)	98.3 (93.4)	88.9 (83.5)
I/σ	8.9 (1.6)	8.9 (1.8)
R_{merge}[b]	0.158 (0.382)	0.151 (0.497)
Wilson *B*-factor B_w[a] (Å^2)	33.2	17.8
R_{cryst}[c]	0.171 (0.23)	0.157 (0.20)
R_{free}[c]	0.205 (0.27)	0.194 (0.24)
estimated coordinate error[a] (Å)	0.150	0.119
rmsd from ideal geometry		
bond lengths (Å)	0.016	0.013
bond angles (deg)	1.46	1.46

[a] For the wild-type *C. reinhardtii* Rubisco structure (PDB code 1GK8), the resolution limit is 1.4 Å, the Wilson *B*-factor 11.8 Å^2, and the estimated coordinate error (based on maximum likelihood calculations) 0.034 Å. [b] $R_{merge} = \sum_h\sum_i|I_i(h) - \langle I_i(h)\rangle|/\sum_h\sum_i I_i(h)$, where I is the observed intensity and $\langle I\rangle$ is the mean intensity of reflection h. [c] $R = \sum_{hkl}||F_o| - |F_c||/\sum_{hkl}|F_o|$, where F_o and F_c are the observed and calculated structure factor amplitudes, respectively. [d] Values in parentheses are for the highest resolution shell.

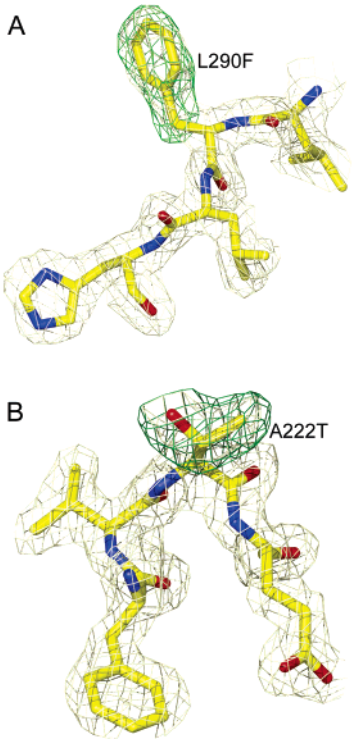

FIGURE 1: Electron density from sigmaA-weighted maps ($2mF_o - DF_c$, gray; $mF_o - DF_c$, green) around the mutant residues Phe290 (A) in the L290F single-mutant enzyme and Thr222 (B) in the L290F/A222T double-mutant enzyme.

Refinement was performed using REFMAC version 5 (*25*). For cross-validation, 5% of the data was excluded from the refinement for R_{free} calculations. Initial electron density maps calculated after one round of rigid body refinement and using data to 3 Å showed clear density for the mutant residues. After building the mutant residues, the mutant structures were further refined using a maximum likelihood target function with noncrystallographic symmetry (NCS) restraints for the eight copies of large and small subunits in the asymmetric unit. Solvent molecules were added using ARP/wARP (*26*). Throughout the refinement, the $2mF_o - DF_c$ and $mF_o - DF_c$ sigmaA-weighted maps (*27*) were inspected and the models manually adjusted using O (*28*). The L290F single-mutant enzyme was refined to final R_{cryst}/R_{free} values of 0.171/0.205 and the L290F/A222T double-mutant enzyme to final values of 0.157/0.194 (Table 1). Volumes of buried cavities were calculated with the program Voidoo (*29*) using a probe radius of 1.0−1.8 Å and a grid spacing of 0.5 Å. Figures were prepared using the programs Molray (*30*) and Pymol (http://www.pymol.org).

RESULTS

Quality and Description of the Structures. The crystallographic data collection and refinement statistics for the mutant enzyme crystal structures are summarized in Table 1. The quality of the structures is evidenced by the low values for R_{cryst} and R_{free} and small deviations from ideal geometry. Initial difference electron density maps for the L290F single-mutant and the L290F/A222T double-mutant enzymes showed clear densities for the substituted residues (Figure 1). Slight shifts of residues surrounding the mutant sites were observed, but no shifts were observed remote from these sites. The final model after refinement comprises residues

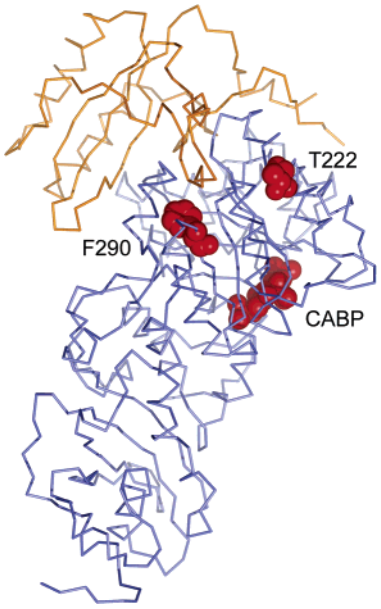

FIGURE 2: Relative positions of the Phe290 and Thr222 substitutions in the L290F/A222T double-mutant enzyme with respect to the transition-state analogue CABP in the large-subunit active site. One large subunit (blue) and one small (yellow) subunit are denoted by ribbons. Phe290, Thr222, and CABP are shown as spheres.

10−475 (from a total of 475 residues) of the large subunits and residues 1−140 (from a total of 140 residues) of the small subunits. Good density was observed for these residues in all subunits of the hexadecamer. This indicates that NCS is followed strictly, as was observed earlier for the wild-type enzyme (*21*). Attempts to relax NCS restraints resulted in increases in the free *R*-factor. This indicated that this operation did not lead to an improvement of the structures and was thus not pursued. Clear density was also observed for the carbamoyl group on Lys201, the metal, and the transition-state analogue CABP. Judged by the electron density, modified residues (Hyp104 and Hyp151, methyl-Cys256 and methyl-Cys369) unique to the *Chlamydomonas* holoenzyme (*21*) are also present in the mutant enzyme structures.

Residue 290 is situated at the beginning of β-strand 5 of the carboxyl-terminal α/β-barrel domain of the large subunit, and its Cα is 18.2 Å away from the catalytically important magnesium ion at the active site (Figure 2). The L290F substitution must therefore affect the relative rates of carboxylation and oxygenation in an indirect way. Residue 222 is positioned roughly in the middle of α-helix 2 of the α/β barrel. Its Cα is 20.0 Å away from the active site magnesium, 15.2 Å (Cα−Cα) away from residue 290 in the same subunit (Figure 2), and 18.7 Å (Cα−Cα) from residue 290 in the nearest neighboring large subunit. Thus the effect of the A222T suppressor substitution must also be indirect.

The shortest interaction path between residues 290 and 222 within the same large subunit (intrasubunit path) is mediated via Pro263 and Val262 (Figure 3). The carbonyl oxygen of Pro263 interacts with residue 290 via main-chain hydrogen bonding and van der Waals contact (side chain). The side chain of Val262 interacts with the side chain of residue 222 at a distance of 4.1 Å in the wild-type and L290F single-mutant enzymes, but in the L290F/A222T double-mutant enzyme, this distance is shortened to 3.5 Å (Cγ−Oγ). An indirect path is also provided via residues in the

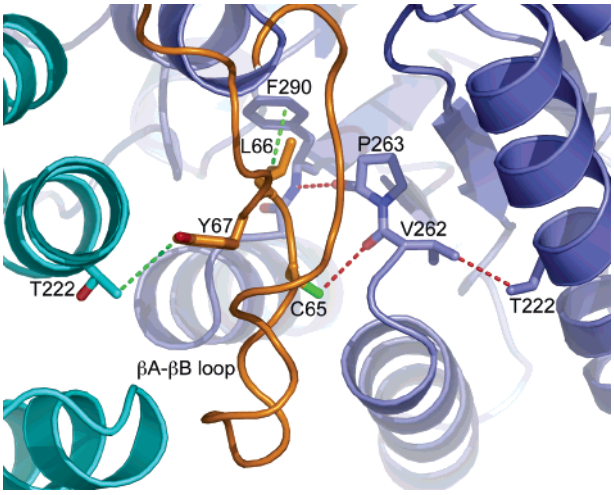

FIGURE 3: Interactions between residues 290 and 222 mediated by residues in large and small subunits. Interactions in only the L290F/A222T double mutant are shown, but similar interactions are also present in the wild-type and L290F single-mutant enzymes. Large subunits are colored slate blue and cyan. The small subunit is colored yellow. Interaction paths are colored red (intrasubunit path) and green (intersubunit path).

small subunit (Figure 3). Here, the side chain of residue 290 makes van der Waals contact with the side chain of Leu66 in the small subunit. The side chain of the preceding small subunit residue, Cys65, interacts with the carbonyl oxygen of Val262, which in turn interacts with Ala222. This interaction is maintained in the double-mutant enzyme (Figure 3). The shortest interaction path between residues 290 and 222 in neighboring large subunits (intersubunit path) involves residues from the small subunit. The 290 side chain makes a van der Waals interaction with the side chain of Leu66 in the small subunit, and the small subunit Tyr67 side chain is within van der Waals bonding distance of Ala222 in the adjacent large subunit. This latter interaction is shortened by the introduction of the bulkier threonine in the L290F/A222T double-mutant enzyme (Figure 3).

Differences That Arise from the Mutant Substitutions. Along the intrasubunit path in the single-mutant enzyme, the side chain of Val262 is slightly shifted toward Phe290 and away from Ala222 (Figure 4B). In the L290F/A222T double-mutant enzyme, the Val262 side chain is restored to the wild-type position. More differences are observed along the intersubunit path via the small subunit. In both the L290F single-mutant and L290F/A222T double-mutant enzymes, the side chain of small-subunit Leu66 is slightly rotated relative to the wild type (Figure 4A). The side chain of Lys161 makes van der Waals contacts with Leu290 in the wild-type enzyme, but in the L290F enzyme, it adopts a slightly different conformation, thereby maintaining the interaction with small-subunit Leu66. In the L290F/A222T double-mutant enzyme, the Thr222 side chain makes an extra hydrogen bond with the main-chain carbonyl of Phe218 at the base of α-helix 2. This helix in turn makes interactions with residues along the intersubunit path. The β-strand and loop preceding α-helix 2 contain the residues (Asp203, Glu204, and carbamylated Lys201) that bind the active site magnesium ion. Thus, differences in interactions with α-helix 2 have the potential for influencing catalysis. Analysis of the interactions between CABP and amino acid residues of the enzyme shows that there are only small shifts in bond lengths in the mutants

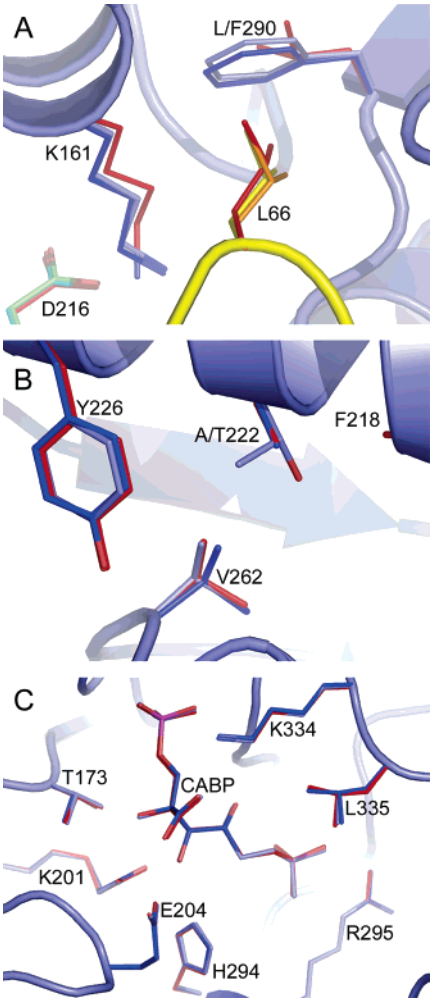

FIGURE 4: Structural differences close to mutant residue 290 (A), suppressor residue 222 (B), and the transition-state analogue CABP in the active site (C). The large subunit is colored blue with side chains colored dark blue in the L290F single mutant and light blue in the L290F/A222T double mutant. The small subunit is colored yellow with the side chain of Leu66 colored yellow in the single mutant and orange in the double mutant. Corresponding side chains in the wild-type enzyme (*21*) are colored red. D216 in panel A is from an adjacent large subunit and is colored green.

relative to the wild type. The largest shift is a lengthening (by 0.3 Å) of the hydrogen bond between the γ-oxygen of Thr173 to O2 of CABP in the L290F mutant structure relative to the L290F/A222T revertant or wild-type structures (Figure 4C).

Leu66 is part of a loop of the small subunit, the βA−βB loop, that displays extensive inter- and intrasubunit interactions. Despite this, no further atom displacements were observed in this loop (but see below). Residue 51 at one end of the loop exists in a dual conformation in the wild-type enzyme (*21*). There are indications in the electron density maps of dual conformations, but because of the lower resolution limits of the mutant structures, Tyr51 was refined as its mean single conformation here.

Another region that shows structural variability between the mutant and wild-type enzymes is located at the carboxyl terminus of the large subunit between residues 438 and 466. This region lies between α-helix 8 of the α/β barrel and the flexible carboxyl terminus that closes over the active site during catalysis (*31*). Although the overall fold is identical, this region also shows small differences between the two

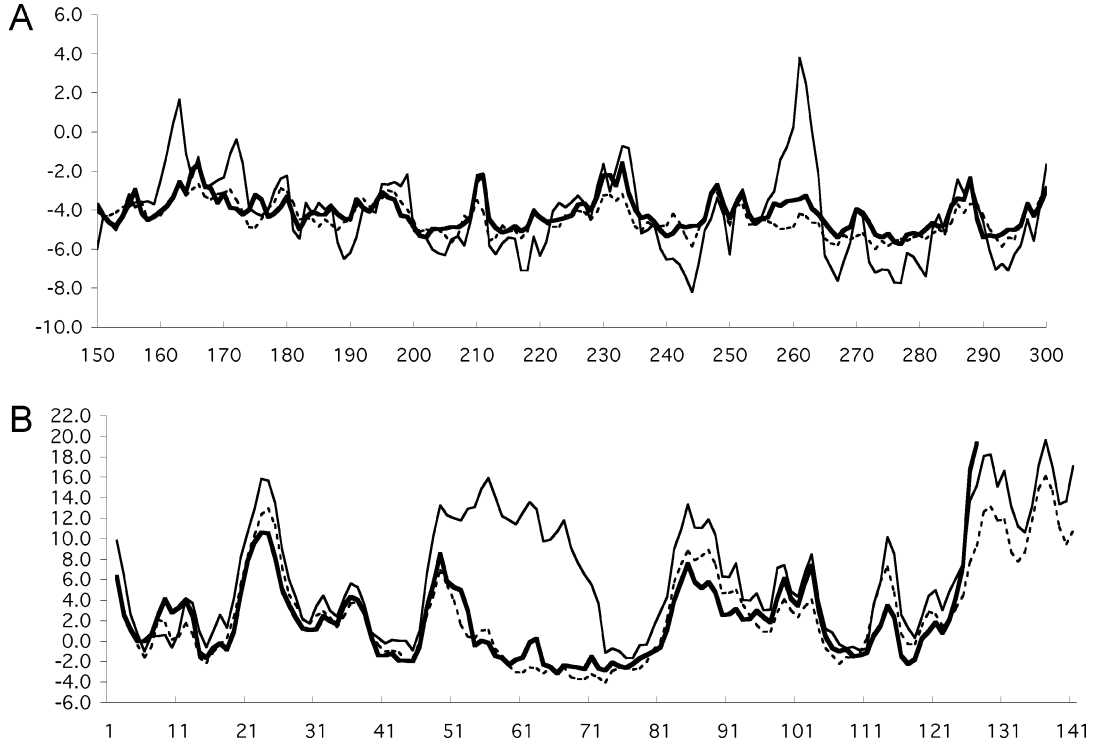

FIGURE 5: Atomic temperature factors (*B*-factors) corrected for crystal disorder: (A) large-subunit residues 150−300 and (B) all small-subunit residues. These values are not corrected for bulk solvent. Key: wild-type, thick line; L290F, thin line; L290F/A222T, dashed line.

reported wild-type *Chlamydomonas* Rubisco structures with PDB codes 1GK8 (*21*) and 1IR2 (*32*). In the former structure, a disulfide bond exists between Cys449 and Cys459. This is also the case in the L290F single-mutant structure but not in the L290F/A222T double-mutant structure. This difference in oxidation state almost certainly contributes to differences observed between the structures. Whether the Cys residues are oxidized or reduced may be due in part to the presence of β-mercaptoethanol rather than dithiothreitol in the purification buffer or as a result of the photoreducing effect of X-rays during data collection from the crystal (*33*). Thus, it is unlikely that the differences observed in this region are caused by the L290F or A222T substitutions.

B-Factor Analysis and Rubisco Thermal Stability. The differences observed at Val262 along the intrasubunit interaction path are consistent with the phenotypes that result from the L290F-mutant and A222T-suppressor substitutions (*18*) whereas the alterations along the intersubunit path that are the same in both the L290F-mutant and L290F/A222T-revertant structures are more likely to arise from only the L290F substitution. It was previously proposed that the intersubunit contacts between large and small subunits, in particular those involving the small-subunit loop between β-strands A and B, may be key interactions both for maintaining catalytic function and for holoenzyme stability (*18*, *19*, *34*). Analysis of the atomic temperature factors of the mutant enzymes compared with the wild-type enzyme supports this hypothesis.

The atomic temperature factor (*B*-factor) of an atom determined by X-ray crystallography is an estimate of the disorder of that atom within the crystal lattice. Two main factors contribute to the magnitude of the *B*-factor. The first is the crystal packing disorder, the Wilson *B*-factor (B_W). This can be estimated from the experimental data from the decay of diffraction intensity with increasing resolution. The second factor is the thermal vibration of each atom within a molecule (B_{therm}). The refined atomic temperature factor B_{atom} is an estimate of the sum $B_W + B_{therm}$ for each atom. Because the data for the wild-type, single-mutant, and double-mutant structures were collected from three different crystals, we can compare estimates of B_{therm} in order to eliminate the crystal-dependent disorder.

B-factor analysis for the mutant and wild-type (PDB code 1GK8) enzymes shows some highly significant differences between the L290F single-mutant structure compared with both the wild-type and double-mutant structures (Figure 5). Residues 50−72 of the small subunit and residues 161−164 and 259−264 of the large subunit show significant and systematically increased *B*-factors in the L290F structure. These regions are concentrated around those residues in which differences are observed between mutant sites (i.e., small-subunit Leu66 and large-subunit Lys161 and Val262) (Figure 6). This effect of the L290F single substitution could explain the temperature-conditional phenotype of the mutant strain because atomic disorder increases with temperature. The mutant enzyme may be sufficiently ordered in these regions to support catalysis at the permissive temperature (25 °C) but not at the restrictive temperature (35 °C). The increased *B*-factors may also explain the observation that Rubisco holoenzyme levels are highly reduced in mutant cells at 35 °C due to increased rates of degradation (*16*, *18*). Disorder at the surface of a protein will expose hydrophobic patches and mimic a misfolded state.

The introduction of the suppressor substitution, A222T, improves the thermal stability and kinetic properties of the original mutant enzyme (*18*, *19*), and the L290F/A222T double-mutant enzyme has *B*-factor values similar to those of the wild-type enzyme (Figure 5). These results indicate that the effect of the V262L suppressor substitution, which also imparts wild-type stability and kinetics to the L290F/

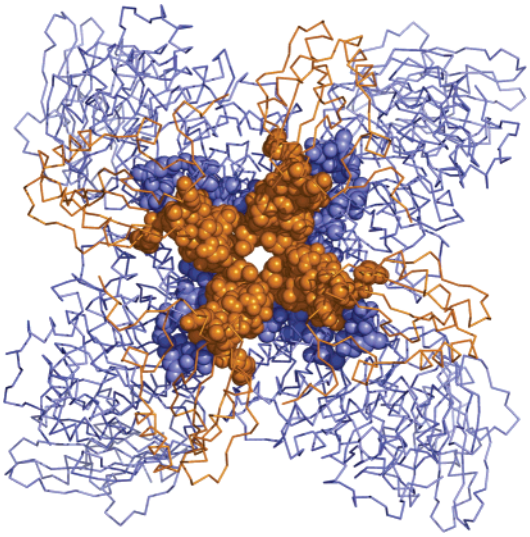

FIGURE 6: Mapping of the region in the large and small subunits that has increased disorder in the single mutant L290F: large subunit, blue; small subunit, yellow. Atoms with increased atomic temperature factors are drawn as spheres.

V262L double-mutant enzyme (*18*, *19*), may be explained by the same phenomenon. Because the side chain of Val262 interacts closely with the side chain of Ala222, it seems probable that replacement of Val262 by the larger Leu residue would have the same effect.

DISCUSSION

Despite variation in catalytic properties (*7*−*9*), Rubisco enzymes from diverse species have nearly identical active site X-ray crystal structures (reviewed in ref *3*), and mutant screening and selection in *Chlamydomonas* have identified several amino acid substitutions far from the active site that influence Ω and carboxylation catalytic efficiency (reviewed in ref *1*). Together, these observations indicate that structural differences relatively far from the site of catalysis can make a substantial contribution to catalytic efficiency and specificity. However, it remains difficult to deduce the means by which distant structural differences influence the active site. In the present study, we have solved the X-ray crystal structures of two mutant Rubisco enzymes of *Chlamydomonas*. The L290F mutant enzyme has decreases in Ω and thermal stability whereas the L290F/A222T revertant enzyme has relatively improved thermal stability and an Ω increased to the wild-type value (*16*−*19*). These large-subunit substitutions occur at residues ∼19 Å from the active site, close to the interface with the small subunit.

At first glance of the X-ray crystal structures, it is difficult to see the reason for the dramatic effects of the L290F substitution on specificity and thermal stability (*16*). It is also not obvious why a second substitution, A222T, should complement the deleterious effects of the original L290F mutant substitution (*18*, *19*). The affected residues are far apart, at a distance of 15 Å, and remote from the active site (∼19 Å from Mg^{2+}). The substitutions cause only minimal changes in structure apart from the replaced residues themselves. No shifts of the Cα backbones or exchanges of side-chain rotamers are apparent.

The replacement of Leu290 by Phe adds bulk in the core of the protein but causes little or no perturbation of the structure globally. No cavities were detected in the vicinity of Leu290 that could accommodate the additional bulk of the phenylalanine side chain. Instead, the introduction of the bulkier Phe side chain is accommodated by the slight shifts of Lys161 of the large subunit and Leu66 of the adjacent small subunit (Figure 4). One might assume that suppression would be achieved by relieving the strain on Phe290 by the introduction of a smaller residue at a second site. However, this is not the case. Second-site suppression is accomplished by the addition of even more bulk at a distance from the L290F mutant substitution. This is the case in the L290F/A222T revertant enzyme investigated here and also in a second revertant of L290F resulting from a V262L suppressor substitution (*18*, *19*). Although the A222T (or V262L) suppressor substitution improves the thermal stability of the L290F mutant enzyme in vitro and in vivo (*18*), it also increases the thermal stability of the wild-type enzyme (*35*). Thus, it is not surprising that a direct interaction between the mutant and suppressor residues is not observed and that improved thermal stability does not necessarily require correction of any structural alterations brought about by the L290F mutant substitution. However, one might expect that the A222T substitution would return some alterations in structure back to those of wild type, considering that A222T improves the Ω value and carboxylation catalytic efficiency of the L290F mutant enzyme but has little effect on the catalytic properties of the wild-type enzyme (*19*).

Improved Rubisco thermal stability seems to be the basis for genetic selection of A222T as a second-site suppressor of the L290F mutant substitution (*19*). In general, amino acids that are branched at the Cβ atom are expected to be destabilizing within an α-helix due to restriction of conformation (*36*). The hydroxyl group of threonine may also have a destabilizing effect owing to its ability to make a hydrogen bond in the unfolded state. However, these effects may be modulated by the structural context of the helix (i.e., whether it is buried or exposed to solvent). In the L290F/A222T enzyme, the side chain of Thr222 makes one intrachain hydrogen bond and a number of additional packing interactions not present in the wild-type enzyme (*21*). These interactions may increase rigidity and thereby improve stability.

In the single-site mutant enzyme, replacement of Leu290 by Phe destabilizes a region of the enzyme that can now be exactly defined by increases in *B*-factors of residues in both the large and small subunits. It is interesting to note that one of the largest effects of the L290F mutation is around residue 262 of the large subunit (Figure 5A), which corresponds to the second suppressor substitution. In the L290F/A222T revertant enzyme, the magnitude of the temperature factors is restored to wild-type levels (Figure 5). Mapping of the effect on the structure (Figure 6) illustrates that, despite being far apart in primary structure, the affected residues form a contiguous volume in the protein. This volume, comprising 4550 $Å^3$, contains residues 50−72 of the small subunit (i.e., the βA−βB loop) and two adjacent regions of the large subunit. Because this region is close to the 4-fold molecular axis of the hexadecameric holoenzyme, regions from eight symmetry-related subunits (four large and four small subunits) together form a volume of considerable size (∼18000 $Å^3$ per interface at each end of the molecule).

The increase in the *B*-factors of small-subunit βA−βB-loop residues correlates well with the observation that substitutions in this loop can complement the L290F substitution in a manner similar to that of A222T (*19*, *35*). Small-subunit N54S and A57V suppressor substitutions, which are distant from L290F and the paths connecting residues 290 and 222 described here (Figures 2 and 3), also improve the catalytic properties and thermal stability of the L290F mutant enzyme (*35*). Furthermore, an R71A directed-mutant substitution in the small-subunit βA−βB loop causes significant decreases in Ω, catalytic efficiency, and holoenzyme thermal stability and results in a temperature-conditional phenotype like that of the L290F large-subunit mutant (*37*). We note that the guanidinium group of Arg71 makes a hydrogen bond to the carbonyl oxygen of small-subunit Leu66 on the intermolecular path (Figure 3) (*21*). It is thus apparent that interactions at the interface between large subunits and small-subunit βA−βB loops play a significant role in holoenzyme stability.

The changes at the small/large-subunit interface must influence Ω and catalytic efficiency at the active site (20 Å away) in an indirect manner. The large *B*-factor increases in the L290F single mutant will likely influence the dynamics of the protein, and these effects will ultimately be transmitted to the active site. One long-range path is through β-strand 5 via His294, which is in hydrogen-bonding distance to CABP (*21*). Leu290 is one of several hydrophobic residues that surround Glu158, which is the first residue of a hydrogen bond network (via His325 and His292) that terminates at active site His327 (*38*). His327 is also within hydrogen-bonding distance to CABP. However, no significant coordinate shifts are observed for these residues relative to the wild-type crystal structure (*21*). This is perhaps not surprising because CABP is a close mimic of the carboxylation transition state and forms an extraordinarily tight complex with Rubisco (binding constant of $\sim 10^{-11}$ M for the spinach enzyme) (*39*). This may at least in part explain the similarity in conformation and bond lengths in the wild-type and mutant structures, which all contain CABP. One of the largest shifts is seen for Thr173, which weakens the hydrogen bond of its side chain with CABP in the L290F structure but not in the wild-type or L290F/A222T structures. Whether this difference can account for differences in catalysis may require the analysis of additional mutant enzyme structures. However, it is interesting to note that whereas Thr173 is conserved in all hexadecameric Rubisco enzymes, this residue is replaced by Ile in the homodimeric, low-Ω enzyme of *Rhodospirillum rubrum* (*40*).

The results presented here indicate that Leu290 is a critical residue in *Chlamydomonas* Rubisco owing to its position at the interface between large and small subunits (Figures 2 and 3). A remaining issue concerns the generality of these interactions. Leu290 is conserved in land plants and green algae but is replaced by Phe in *R. rubrum* Rubisco. Ala222 is conserved in land plants and *R. rubrum*, whereas *Ralstonia eutropha* and *Chromatium vinosum* have Met (*38*). One interaction pathway between the mutant substitution at residue 290 and the suppressor substitution at residue 222 is via residues of the small-subunit βA−βB loop (Figure 3). Perhaps *R. rubrum* Rubisco has a different residue at position 290 because it lacks small subunits, further indicating that the small-subunit βA−βB loop has a critical influence over large-subunit structure in hexadecameric Rubisco. It is also worth pointing out that the βA−βB loop differs substantially among divergent Rubisco enzymes. It is comprised of 28 residues in green algae and ∼22 residues in land plants but only 10 residues in prokaryotes and nongreen algae (reviewed in ref *11*). In nongreen algae and some prokaryotes, a longer carboxyl terminus of the small subunit forms a β-hairpin structure that takes the place of the missing βA−βB-loop residues (*41*, *42*). Considering that directed-mutant substitutions in the *Chlamydomonas* large and small subunits at this subunit interface can influence Ω and catalytic efficiency (*35*, *37*), it seems possible that structural diversity of the small-subunit βA−βB loop may contribute to the differences in catalytic properties of divergent Rubisco enzymes (*7*−*9*). Structural analysis of the mutant enzymes in the present study provides a physical basis for intersubunit interactions in the region of the small-subunit βA−βB loop and indicates that further investigation of this region is warranted with respect to Rubisco improvement.

ACKNOWLEDGMENT

We thank Andreas Cederlund for excellent technical assistance.

REFERENCES

1. Spreitzer, R. J., and Salvucci, M. E. (2002) Rubisco: Structure, regulatory interactions, and possibilities for a better enzyme, *Annu. Rev. Plant Biol. 53*, 449−475.
2. Parry, M. A. J., Andralojc, R. A. C., Mitchell, P. J., Madgwick, P. J., and Keys, A. J. (2003) Manipulation of Rubisco: the amount, activity, function and regulation, *J. Exp. Bot. 54*, 1321−1333.
3. Andersson, I., and Taylor, T. C. (2003) Structural framework for catalysis and regulation in ribulose-1,5-bisphosphate carboxylase/oxygenase, *Arch. Biochem. Biophys. 414*, 130−140.
4. Andrews, T. J., and Whitney, S. M. (2003) Manipulating ribulose bisphosphate carboxylase/oxygenase in the chloroplasts of higher plants, *Arch. Biochem. Biophys. 414*, 159−169.
5. Laing, W. A., Ogren, W. L., and Hageman, R. H. (1974) Regulation of soybean net photosynthetic CO_2 fixation by the interaction of CO_2, O_2, and ribulose 1,5-diphosphate carboxylase, *Plant Physiol. 54*, 678−685.
6. Spreitzer, R. J. (1999) Questions about the complexity of chloroplast ribulose-1,5-bisphosphate carboxylase/oxygenase, *Photosynth. Res. 60*, 29−42.
7. Jordan, D. B., and Ogren, W. L. (1981) Species variation in the specificity of ribulose biphosphate carboxylase/oxygenase, *Nature 291*, 513−515.
8. Read, B. A., and Tabita, F. R. (1994) High substrate-specificity factor ribulose-bisphosphate carboxylase oxygenase from eukaryotic marine-algae and properties of recombinant cyanobacterial rubisco containing algal residue modifications, *Arch. Biochem. Biophys. 312*, 210−218.
9. Uemura, K., Anwaruzzaman, Miyachi, S., and Yokota, A. (1997) Ribulose-1,5-bisphosphate carboxylase/oxygenase from thermophilic red algae with a strong specificity for CO_2 fixation, *Biochem. Biophys. Res. Commun. 233*, 568−571.
10. Dean, C., Pichersky, E., and Dunsmuir, P. (1989) Structure, evolution, and regulation of *RbcS* genes in higher-plants, *Annu. Rev. Plant Physiol. Plant Mol. Biol. 40*, 415−439.
11. Spreitzer, R. J. (2003) Role of the Rubisco small subunit, *Arch. Biochem. Biophys. 414*, 141−149.
12. Roy, H., and Andrews, T. J. (2000) in *Photosynthesis: Physiology and metabolism* (Leegood, R. C., Sharkey, T. D., and von Caemmerer, S., Eds.) pp 53−83, Kluwer Academic Publishers, Dordrecht, The Netherlands.
13. Kanevski, I., Maliga, P., Rhoades, D. F., and Gutteridge, S. (1999) Plastome engineering of ribulose-1,5-bisphosphate carboxylase/oxygenase in tobacco to form a sunflower large subunit and tobacco small subunit hybrid, *Plant Physiol. 119*, 133−141.

14. Whitney, S. M., von Caemmerer, S., Hudson, G. S., and Andrews, T. J. (1999) Directed mutation of the Rubisco large subunit of tobacco influences photorespiration and growth, *Plant Physiol. 121*, 579−588.
15. Hartman, F. C., and Harpel, M. R. (1994) Structure, function, regulation, and assembly of D-ribulose-1,5-bisphosphate carboxylase oxygenase, *Annu. Rev. Biochem. 63*, 197−234.
16. Chen, Z., Chastain, C. J., Al-Abed, S. R., Chollet, R., and Spreitzer, R. J. (1988) Reduced CO_2/O_2 specificity of ribulose-bisphosphate carboxylase/oxygenase in a temperature-sensitive chloroplast mutant of *Chlamydomonas*, *Proc. Natl. Acad. Sci. U.S.A. 85*, 4696−4699.
17. Chen, Z., Hong, S., and Spreitzer, R. J. (1993) Thermal-instability of ribulose-1,5-bisphosphate carboxylase oxygenase from a temperature-conditional chloroplast mutant of *Chlamydomonas reinhardtii*, *Plant Physiol. 101*, 1189−1194.
18. Hong, S., and Spreitzer, R. J. (1997) Complementing substitutions at the bottom of the barrel influence catalysis and stability of ribulose-bisphosphate carboxylase/oxygenase, *J. Biol. Chem. 272*, 11114−11117.
19. Du, Y. C., and Spreitzer, R. J. (2000) Suppressor mutations in the chloroplast-encoded large subunit improve the thermal stability of wild-type ribulose-1,5-bisphosphate carboxylase/oxygenase, *J. Biol. Chem. 275*, 19844−19847.
20. Spreitzer, R. J., and Mets, L. (1981) Photosynthesis-deficient mutants of *Chlamydomonas reinhardt*ii with associated light-sensitive phenotypes, *Plant Physiol. 67*, 565−569.
21. Taylor, T. C., Backlund, A., Björhall, K., Spreitzer, R. J., and Andersson, I. (2001) First crystal structure of Rubisco from a green alga−*Chlamydomonas reinhardtii*, *J. Biol. Chem. 276*, 48159−48164.
22. Otwinowski, Z., and Minor, W. (1997) Processing of X-ray diffraction data collected in oscillation mode, *Methods Enzymol. 276*, 307−326.
23. Navaza, J., and Saludjian, P. (1997) AMoRe: An automated molecular replacement program package, *Methods Enzymol. 276*, 581−594.
24. Collaborative Computational Project, Number 4 (1994) The CCP4 suite−programs for protein crystallography, *Acta Crystallogr. D50*, 760−763.
25. Murshudov, G. N., Vagin, A. A., and Dodson, E. J. (1997) Refinement of macromolecular structures by the maximum-likelihood method, *Acta Crystallogr. D53*, 240−255.
26. Perrakis, A., Sixma, T. K., Wilson, K. S., and Lamzin, V. S. (1997) wARP: Improvement and extension of crystallographic phases by weighted averaging of multiple-refined dummy atomic models, *Acta Crystallogr. D53*, 448, 659−455.
27. Pannu, N. S., and Read, R. J. (1996) Improved structure refinement through maximum likelihood, *Acta Crystallogr. A52*, 659−668.
28. Jones, T. A., Zou, J.-Y., Cowan, S. W., and Kjeldgaard, M. (1991) Improved methods for building protein models in electron-density maps and the location of errors in these models, *Acta Crystallogr. A47*, 110−119.
29. Kleywegt, G. J., and Jones, T. A. (1994) Detection, delineation, measurement and display of cavities in macromolecules, *Acta Crystallogr. D50*, 178−185.
30. Harris, M., and Jones, T. A. (2001) Molray−a web interface between O and POV-Ray ray tracer, *Acta Crystallogr. D57*, 1201−1203.
31. Taylor, T. C., and Andersson, I. (1997) The structure of the complex between rubisco and its natural substrate ribulose-1,5-bisphosphate, *J. Mol. Biol. 265*, 432−444.
32. Mizohata, E., Matsumura, H., Okano, Y., Kumei, M., Takuma, H., Onodera, J., Kato, K., Shibata, N., Inoue, T., Yokota, A., and Kai, Y. (2002) Crystal structure of activated ribulose-1,5-bisphosphate carboxylase/oxygenase from green alga *Chlamydomonas reinhardtii* complexed with 2-carboxyarabinitol-1,5-bisphosphate, *J. Mol. Biol. 316*, 679−691.
33. Weik, M., Ravelli, R. B. G., Kryger, G., McSweeney, S., Raves, M. L., Harel, M., Gros, P., Silman, I., Kroon, J., and Sussman, J. L. (2000) Specific chemical and structural damage to proteins produced by synchrotron radiation, *Proc. Natl. Acad. Sci. U.S.A. 97*, 623−628.
34. Du, Y. C., Peddi, S. R., and Spreitzer, R. J. (2003) Assessment of structural and functional divergence far from the large-subunit active site of ribulose-1,5-bisphosphate carboxylase/oxygenase, *J. Biol. Chem. 278*, 49401−49405.
35. Du, Y. C., Hong, S., and Spreitzer, R. J. (2000) RbcS suppressor mutations improve the thermal stability and CO_2/O_2 specificity of rbcL-mutant ribulose-1,5-bisphosphate carboxylase/oxygenase, *Proc. Natl. Acad. Sci. U.S.A. 97*, 14206−14211.
36. Blaber, M., Zhang, X. J., Lindstrom, J. D., Pepiot, S. D., Baase, W. A., and Matthews, B. W. (1999) Determination of α-helix propensity within the context of a folded protein, *J. Mol. Biol. 235*, 600−624.
37. Spreitzer, R. J., Esquivel, M. G., Du, Y. C., and McLaughlin, P. D. (2001) Alanine-scanning mutagenesis of the small-subunit βA-βB loop of chloroplast ribulose-1,5-bisphosphate carboxylase/oxygenase: Substitution at Arg-71 affects thermal stability and CO_2/O_2 specificity, *Biochemistry 40*, 5615−5621.
38. Knight, S., Andersson, I., and Brändén, C.-I. (1990) Crystallographic analysis of ribulose 1,5-bisphosphate carboxylase from spinach at 2.4 Å resolution: subunit interactions and the active site, *J. Mol. Biol. 215*, 113−160.
39. Pierce, J., Tolbert, N. E., and Barker, R. (1980) Interaction of ribulosebisphosphate carboxylase/oxygenase with transition-state analogues, *Biochemistry 19*, 934−942.
40. Andersson, I., Knight, S., Schneider, G., Lindqvist, Y., Lundqvist, T., Brändén, C. I., and Lorimer, G. H. (1989) Structure of the active site of ribulose-bisphosphate carboxylase, *Nature 337*, 229−234.
41. Hansen, S., Burkow Vollan, V., Hough, E., and Andersen, K. (1999) The crystal structure of Rubisco from *Alcaligenes eutrophus* reveals a novel central eight-stranded β-barrel formed by β-strands from four subunits, *J. Mol. Biol. 288*, 609−621.
42. Sugawara, H., Yamamoto, H., Shibata, N., Inoue, T., Okada, S., Miyake, C., Yokota, A., and Kai, Y. (1999) Crystal structure of carboxylase reaction-oriented ribulose-1,5-bisphosphate carboxylase/oxygenase from a thermophilic red alga, *Galdieria partita*, *J. Biol. Chem. 274*, 15655−15661.

BI047928E